ACS OMEGA

http://pubs.acs.org/journal/acsodf

Article

Glucose Sensing in Human Whole Blood Based on Near-Infrared Phosphors and Outlier Treatment with the Programming Language "R"

Hsia-An Lee, Peng-Yi Lin, Anastasia I. Solomatina, Igor O. Koshevoy, Sergey P. Tunik,* Hui-Wen Lin,* Sheng-Wei Pan,* and Mei-Lin Ho*

Cite This: *ACS Omega* 2022, 7, 198−206

Read Online

ACCESS | Metrics & More | Article Recommendations | Supporting Information

ABSTRACT: A near-infrared paper-based analytical device (**NIR-PAD**) for glucose detection in whole blood was based on iridium(III) metal complexes embedded in a three-dimensional (3D) enzyme gel. These complexes emit NIR luminescence, can avoid interference from the color of blood, and increase the sensitivity of sensing glucose. The glucose reaction behaviors of another two different iridium(III) and platinum(II) complexes were also tested. When the glucose solution was added to the device, the oxidation of glucose by glucose oxidase caused oxygen consumption and increased the intensity of the phosphorescence emission. To the best of our knowledge, this is the first time that data have been treated with the programming language "R", which uses Tukey's test to identify the outliers in the data and calculate a median for establishing a calibration curve, in order to improve the accuracy of **NIR-PADs** for sensing glucose. Compared with other published devices, **NIR-PADs** exhibit a wider linear range (1−30 mM, [relative emission intensity] = 0.0250[glucose] + 0.0451, and R^2 = 0.9984), a low detection limit (0.7 mM), a short response time (<2 s), and a small sample volume (2 μL). Finally, blood specimens were obtained from 19 patients enrolled in Taipei Veterans General Hospital under an approved IRB protocol (Taiwan; 2017-12-002CC). The sensors exhibited remarkable characteristics for glucose detection in comparison with other methods, including the clinical method in hospitals as well as those without blood sample pretreatment or a dilution factor. The above results confirm that **NIR-PAD** sensors can be put to practical use for glucose detection.

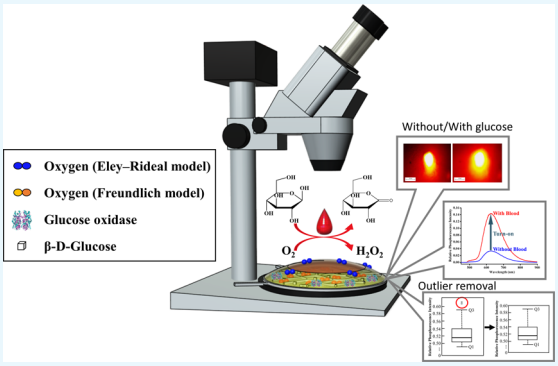

INTRODUCTION

Nowadays, about 463 million people in the world have diabetes mellitus, which is a common metabolic disease and can induce complications such as kidney failure, vision loss, and myocardial infarction.[1−3] Optical sensing, which is a fast, highly precise, non-invasive, and non-destructive analytical tool, is extremely useful in experimental and practical medicine for the analysis of various pathologies. In this respect, the use of sensors with near-infrared (NIR) emission (650−950 nm) is much more convenient than using their counterparts that emit in the visible region due to advantages such as lower surface tissue/blood absorption, reduced scattering, greater penetration depth, and weaker sensor signal interference with background fluorescence.[4,5] Blood is not transparent to visible light because reflective light is interfered with by a hemochrome. Therefore, NIR phosphors and NIR spectroscopy possess great potential to facilitate the observation of molecular biotargets in cells and deep tissues.

Recently, Liu et al. have applied an upconversion nanoparticle polydopamine optical sensor to detect glucose in human serum and whole blood. The sensor response is generated by emission quenching using hydrogen peroxide (H_2O_2) produced from the glucose oxidase (GOx)/glucose enzymatic reaction under NIR excitation.[2] Yu et al. suggested a NIR ratiometric fluorescent probe, whose sensor properties are based on a similar chemistry where the fluorescence of the NIR quantum dots is quenched upon an increase in glucose concentration.[6] In both cases,[2,6] increases in glucose levels cause emission reduction, whereas for analytical methodology, the turn-on-type luminescence systems are substantially more sensitive than the turn-off ones.[7] Therefore, Deng et al. used NIR fluorescent nanoprobes (iRGMs) to detect glucose in whole blood, in which the fluorescence of iRGMs was quenched by MnO_2 via energy transfer. When the iRGMs were mixed with the whole blood, GO*x* converted blood glucose into gluconic acid and H_2O_2 and the latter reduced

Received: August 13, 2021
Accepted: December 9, 2021
Published: December 20, 2021

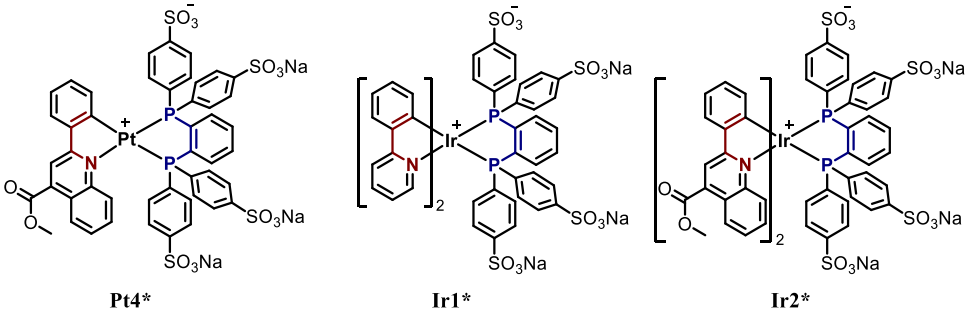

Figure 1. Structures of **Pt4***, **Ir1***, and **Ir2***.

MnO_2, thus increasing the fluorescence of iRGMs.[8] On the other hand, conventional fluorescence bioprobes such as quantum dots and organic dyes frequently suffer from interference with the autofluorescence of biomolecules, low photochemical stability, and high toxicity.[9,10] Phosphorescent probes have attracted considerable interest due to their high two-photon absorption cross sections and the relatively long lifetimes, which enable discrimination of the probe emission from background fluorescence and other short-time luminescent signals by time-gated measurements.[10,11]

A large number of NIR phosphorescent emitting dyes have been developed in recent years as promising chemical sensors and bioimaging probes. Of particular interest are transition-metal complexes (e.g., containing Pt and Ir ions as core metal centers), which display high quantum yields and excellent color adjustability due to strong metal-induced spin−orbit coupling and easy variations in the structure and properties of the ligand environment.[11−15] Li et al. reported a novel NIR phosphorescent iridium(III) complex (FNO2) probe which is suitable for *in vivo* imaging to detect peroxynitrite. The sensing mechanism can be described in the following way: A strong electron-withdrawing group, 2,4-dinitroaniline, is introduced into one of the ligands to quench the probe luminescence. The reaction of the complex with peroxynitrite removes 2,4-dinitroaniline within seconds, and the luminescence intensity of the probe is increased.[16] Zhang et al. combined polydopamine nanoparticles with NIR phosphorescent iridium(III) complexes and applied them to imaging of intracellular pH values in the skin.[17] These examples[16,17] clearly demonstrated that the application of iridium phosphors with a large Stokes shift and a long luminescence lifetime help to avoid the interference with background autofluorescence and give higher sensitivity and resolution in biological imaging.

As for the other NIR complexes, Zach and co-workers presented a couple of NIR phosphorescent platinum(II) complexes and their application in a glucose optode for measuring the internal oxygen gradient subcutaneously. The glucose optode is composed of a first complex layer, GO*x*, a diffusion barrier, and a second complex layer, giving rise to the difference in the composition of oxygen gas values (pO_2). The obtained signal of the sensor corresponding to the glucose levels is the difference between the oxygen levels (ΔpO_2) measured by two oxygen sensors.[18] Importantly, optical detection of glucose in whole blood is still challenging, and conventional UV−vis fluorescence complexes are not suitable for subcutaneous measurement. However, phosphorescent complexes in the NIR optical window can overcome this limitation. Previously, we synthesized a series of cyclometalated Pt(II) and Ir(III) complexes containing auxiliary sulfonated diphosphine (bis(diphenylphosphino) benzene (dppb*). The complexes are water soluble with high two-photon absorption cross sections and have superior sensitivity for oxygen.[11] However, their application to the study of biological samples has not been widely developed yet.

On the other hand, outliers and missing values are frequently encountered during the data collection and computer processing stages. Outliers significantly affect statistics (e.g., the average and standard deviation of a sample) for they may result in values that are sufficiently overestimated or underestimated, distorting group results and compromising the statistical utility and reliability of the study.[19] Therefore, identifying outliers and missing values is a momentous problem in various fields of research and has important applications in medical research.[20,21] Wang and co-workers have applied programming software in R to outlier identification and treatment of mislabeled omics data.[22] Estiri et al. developed an unsupervised clustering-based anomaly/outlier detection approach for detecting implausible observations in Electronic Health Records.[23] In addition, the use of paper-based devices as biosensors has become attractive for point-of-care devices.[24−34]

In the present work, cyclometalated Pt(II) and Ir(III) complexes[11] (**Pt4***, **Ir1***, and **Ir2***, Figure 1) were applied to glucose detection in human whole blood. These compounds have several advantages in glucose detection, such as water solubility, good sensitivity for oxygen, and emission close to the NIR region. Moreover, the detection devices based on these compounds were assembled and applied to the analysis of non-diabetic and diabetic blood. In addition, we used the programming language R to process collected data to construct the calibration curve for glucose detection, for which the outliers in the pretreated data were identified and removed. In this paper, the results of our analytical studies and the data from clinical measurements on human blood are analyzed and discussed, and conclusions are provided.

RESULTS AND DISCUSSION

The cyclometalated Pt(II) and Ir(III) complexes **Pt4*** and **Ir2***, based on sulfonated dppb* ligands, display excellent solubility in water, and the phosphorescent emission maximum is close to the "window of transparency" of biological tissues. Note that a considerable part of their emission band profiles falls into the wavelength range >650 nm (Figure S1) that fits well the first NIR interval and makes it possible to detect emission signal exactly in the "window of transparency" possible. For fair comparison, both compounds have been selected for application in human blood glucose sensing. **Ir1*** also comprises the same dppb*, but its orthometalating ligand contains less-developed aromatic system that results in the

https://doi.org/10.1021/acsomega.1c04344
ACS Omega 2022, 7, 198−206

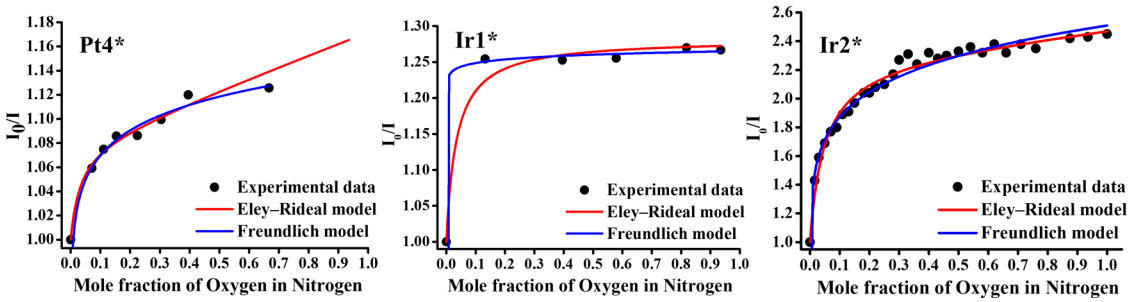

Figure 2. Luminescence quenching of **Pt4***, **Ir1***, and **Ir2*** complexes on paper vs different partial pressures of oxygen and fitting of the data by eqs 1 and 2.

Table 1. Oxygen Quenching Fitting Parameters of Pt4*, Ir1*, and Ir2* on Paper and Comparison of the Oxygen Sensing Performances of the Two Models and Other Recent Published Complexes

	Eley–Rideal model			Freundlich model			
complex	K_{SV1} (atm^{-1})	K_{SV2} (atm^{-1})	R^2	$1/n$	K_f	R^2	refs
Pt4*				0.03	1.14	0.8932	our work
Ir1*				<0.01	1.26	0.8881	our work
Ir2*	0.10 (f_1 = 0.43)	48.72 (f_2 = 0.57)	0.9796	0.13	2.51	0.9921	our work
Ag3	47.60 (f_1 = 0.94)	2.63 (f_2 = 0.06)	0.9915				our previous work[38]
PdOEP–PMMA[a]	18.56 (f_1 = 0.98)	−0.15 (f_2 = 0.02)	0.9999				ref 39

[a]PdOEP–PMMA: palladium octaethylporphine–poly(methylmethacrylate). The unit of *K*sv reported in ref 39 has been converted to atm^{-1}.

emission band shift into the visible region. However, this complex has a larger dynamic range of lifetime, a higher quantum yield, and a good two-photon absorption cross section in aqueous solution. For this reason, it has also been studied for comparison with **Pt4*** and **Ir2*** in the sensing of oxygen in the solid state.

The emission band profiles in the solid state are nearly identical to those obtained in solution,[11] and therefore, the observed emission can be assigned to a combination of metal-perturbed ^{3}IL and ^{3}MLCT excited states with dominating contribution of the former in the case of **Ir1***, whereas the latter gives much larger contribution in the emission of **Pt4*** and **Ir2***. To minimize the absorption and scattering by biomolecules, for example, hemoglobin, compared to short-wavelength light, a longer excitation wavelength, that is, 406 nm, was applied to study the oxygen sensing properties in further sections and in glucose sensing in real samples.

The oxygen quenching experiment was performed to obtain the collision ability between the title compounds and oxygen. The emission intensities of all the three compounds on paper-based cellulose were quenched by different partial pressures of oxygen, and the nonlinear phosphorescence quenching plots (I/I_0) were fitted by two models, namely, the Eley–Rideal model and the Freundlich model, as shown in Figure 2.[35]

The Eley–Rideal model is a two-site model and describes a reaction between an absorbed phosphor and another vapor oxygen which has not chemisorbed on the phosphor. The mechanism assumes that the phosphors are in two different environments and quenched by oxygen at different rates, as expressed in eq 1[35]

$$\frac{I}{I_0} = \frac{f_1}{1 + K_{SV1}[O_2]} + \frac{f_2}{1 + K_{SV2}[O_2]}, \qquad f_1 + f_2 = 1 \tag{1}$$

where I_0 and I denote the emission intensities at the peak maxima under pure nitrogen and different partial pressures of oxygen, respectively, and f_1 and f_2 are the fractions of the total emission intensity generated by each environment, respectively. K_{SV1} and K_{SV2} are the Stern–Volmer quenching constants for each environment.

On the other hand, the dynamic quenching in cellulose paper can be described by the Freundlich model.[36] The diffusional quenching by absorbed oxygen with absorbed phosphors, in which the phosphors in the two sites have different unquenched contributions to the emission intensity and emission intensity ratio, is fitted by eq 2:

$$\frac{I}{I_0} = K_f[O_2]^{1/n} \tag{2}$$

where K_f represents the adsorption capacity and n is an empirical parameter related to the intensity of the adsorption. The same excitation wavelength (406 nm) is applied at **Ir2***, **Ir1***, and **Pt4***, and their fitting parameters are tabulated in Table 1.

As shown in Figure 2 and Table 1, the absorbed surfaces of compounds **Pt4***, **Ir1***, and **Ir2*** are heterogeneous. Regarding **Pt4*** and **Ir1***, the Freundlich model fits the oxygen quenching behavior of **Pt4*** and **Ir1*** much better, which indicates multilayer oxygen adsorption onto an energy-dependent heterogeneous surface. In the case of complex **Ir2***, however, both models were found to match well with the measured quenching results, indicating that both quenching models are involved in oxygen quenching in complex **Ir2***. The Freundlich parameter n values of **Pt4***, **Ir1***, and **Ir2*** all being >1 indicate that oxygen has a good adsorptive property on the surface and presents for further adsorption, representing nonlinear heterogeneous adsorption.[37] The K_f values are in the order of **Ir2*** > **Ir1*** > **Pt4***, showing that **Ir2*** has a higher adsorption capacity for oxygen. This also suggests that **Ir2***, in comparison to **Ir1*** and **Pt4***, has higher ability to sense oxygen, that is, a higher I_0/I value. As shown in Figure 2, the optimal mole fractions of oxygen in nitrogen for **Pt4***, **Ir1***, and **Ir2*** were about 0.08, 0.01, and 0.10, respectively.

https://doi.org/10.1021/acsomega.1c04344
ACS Omega 2022, 7, 198−206

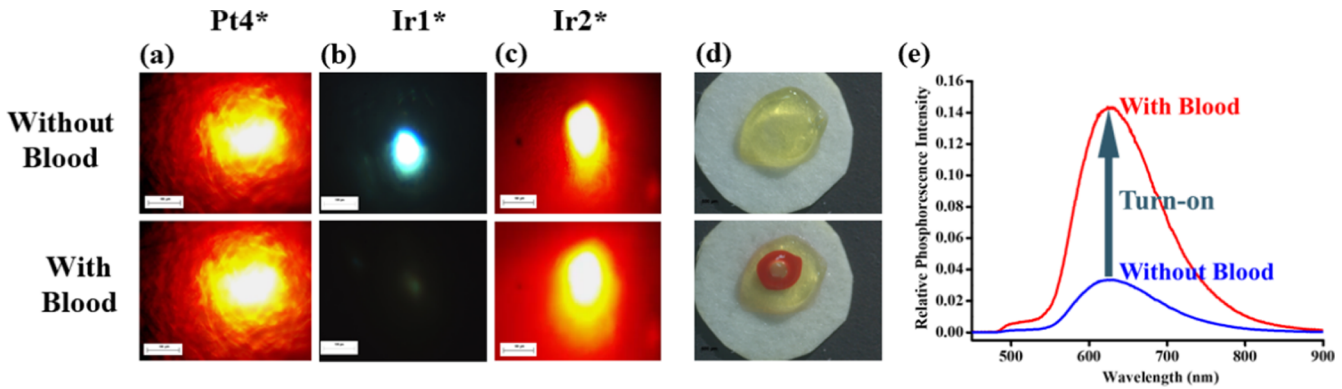

Figure 3. Photographic images of (a–c) **Pt4***, **Ir1***, and **Ir2*** complexes with gel-paper-based sensors upon excitation at 406 nm with/without glucose (4.56 mM), (d) **NIR-PADs** based on **Ir2*** without/with the addition of human blood with diabetes, and (e) luminescence spectra of the **NIR-PADs** before/after adding blood containing glucose (4.56 mM). The scale bar of photographic images (a–c) is 100 μm; scale bar of image (d) is 500 μm.

The quenching constants for the Eley–Rideal model of **Ir2*** indicate that nearly half of the phosphors (43%) were quenched by the quenching constant K_{SV1} = 0.10 atm^{-1}, and nearly 57% were affected by the quenching rate K_{SV2} = 48.7 atm^{-1}. The K_{SV2} value of the quenching constant indicates that 57% of the phosphors were affected by oxygen. Comparing the oxygen sensor data at the two sites with the recently reported quenching rate constants, the **Ir2*** described here has a bigger K_{SV} value, one that exceeds those of phosphorescent oxygen sensors.[38,39] It can function as a sensitive O_2 sensor and can be applied to glucose sensing in human blood (*vide infra*).

During the preparation of **NIR-PADs**, the conditions of each component of the 3D sensing gel, including the amounts of sodium alginate and calcium chloride, the pH value, the concentration of the buffer solution, and the amount of the enzyme, were optically determined. Sodium alginate and calcium chloride are widely used natural polymers due to their environmentally friendly properties; they are nontoxic, low in cost, and biodegradable.[40] The gel of sodium alginate was ionically cross-linked with calcium ions. Sodium alginate with 0.2 M $CaCl_2$ of 35, 40, and 45 mg/mL was tested. For this measurement, the **Ir2*** complex solution, glucose oxidase, buffer concentration, and pH were fixed at 10^{-3} M, 10 mg, 50 mM, and 7, respectively. As shown in Figure S2a, the relative emission intensity upon addition of 0.2 M glucose was measured. When the amount of sodium alginate was 40 mg/mL, the relative emission intensity against glucose had good performance.

Based on a previous study, the gelation speed and hardness are directly proportional to the concentration of calcium.[41] As the amount of $CaCl_2$ increased from 0.2 to 0.6 M and sodium alginate was fixed at 40 mg/mL, as can be seen from Figure S2b, the relative intensity increased gradually, and at 0.5 M, the emission intensity reached its maximum. This is attributable to the gel, which has a suitable hardness, can fix the enzyme, and allows glucose to react with the enzyme.

To test the effect of pH on the detection of glucose, we varied the pH of the buffer solution from pH 5.0 to pH 8.0. As shown by the results in Figure S2c, in the sensing of glucose with buffer solutions of different pH values, the emission intensity increased with increases in the pH of the buffer solution. The increased emission intensity reached the maximum at pH 6.

The concentration of the buffer solution was varied from 5 to 150 mM, as depicted in Figure S2d. This figure reveals that glucose in 10 mM buffer at pH 6 had better ionic strength and the greatest increase in intensity. Figure S2e shows the effects of the amount of enzyme, revealing that the biggest increase in emission intensity occurred in glucose oxidase of 14 mg/mL. All the obtained values above were used in the optimization of **NIR-PADs**.

All of the optimized parameters for the **NIR-PADs** are shown in Table S1. 3D gel was used to encapsulate the enzyme and phosphors, which were measured using fiber optic spectroscopy. Analyte glucose in human blood will react with the oxygen in the gel via glucose oxidase. The consumed vapor oxygen and the reduction of the adsorbed oxygen in the reaction will reduce the dynamic quenching with phosphors, thereby enhancing the overall emission intensity of the **NIR-PADs**. The increase in the emission intensity of the phosphorescence will be proportional to the glucose concentration. The glucose concentration can be calculated using the increase in emission intensity.

Based on the absorption spectra of hemoglobin and oxyhemoglobin, the main absorption peaks are in the spectral range of <600 nm.[42] When the luminescence band is located at this wavelength, the assay is prone to less interference from the biomolecules. Figure 3 presents the photographic images of the **Pt4***, **Ir1***, and **Ir2*** complexes with gel-paper-based sensors without/with blood samples containing 4.56 mM glucose. As shown in Figure 3a–c, the relative brightness changes in the photographs based on the increase of the three phosphors in the **Pt4***- and **Ir2***-based devices and was significantly enhanced in the **Ir2***-based device. Also, the visual change of the **Ir2***-gel-based device (**NIR-PAD**) is shown in Figure 3d. Unlike those of the **Pt4***- and **Ir2***-gel-based devices, the emission intensity of the **Ir1***-based gel device changed upon addition of blood glucose. The emission intensity was quenched due to the emitted visible light being absorbed by hemoglobin and penetrating the blood less (*vide supra;* see also Figure S1). A further comparison of emission intensity changes upon addition of diabetes blood containing 4.56 mM glucose was made between the **Pt4***- and **Ir2***-gel-based devices (**NIR-PADs**). Both complexes emitted close to NIR emission. The emission of **Pt4*** increased by 1.54 folds and 4.28 folds for the **NIR-PADs**, respectively. Hence, the **NIR-PAD** was chosen as the glucose sensing device for the human blood measurement.

https://doi.org/10.1021/acsomega.1c04344
ACS Omega 2022, 7, 198–206

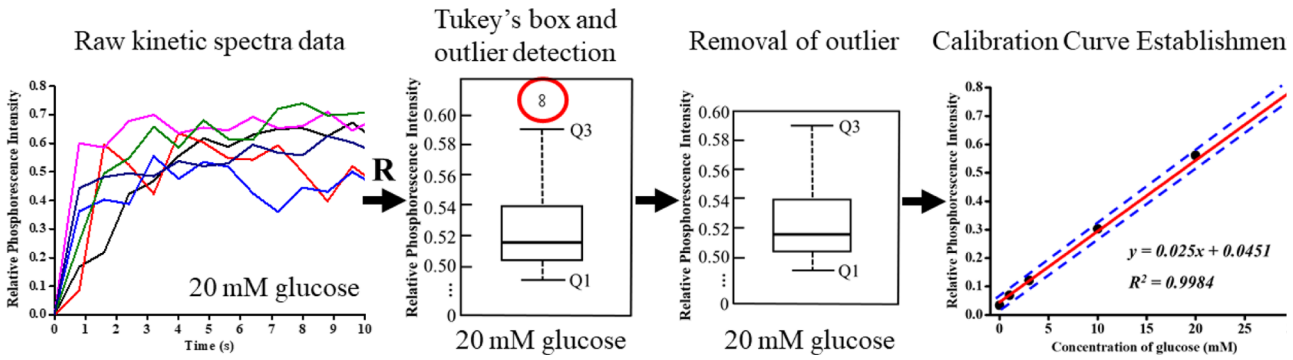

Figure 4. Block diagram showing the data collection and processing via outlier detection and removal to establish the calibration curve for glucose sensing. The red circle is an outlier; the blue dashed line is 95% confidence interval. Taking 20 mM glucose as an example, the data were analyzed between 2 and 10 s.

Table 2. Comparison of Analytical Performances of Recent Direct Glucose Detection Sensors

glucose sensor	methodology	sample types	linear range (mM)	LOD (mM)	sample volume (μL)	response time (s)	refs
iRFP-GO*x*-MnO_2 nanoparticles[a]	fluorescence	whole blood	3.9−8.6	not available	5	10	8
GO*x*@Au@$MagSiO_2$[b]	colorimetric	whole blood	0.44−17.78	0.66	460	1200	43
NIR-PADs	phosphorescence	whole blood	1.0−30.0	0.7	2	2	our work

[a]iRFP-GO*x*-MnO_2 nanoparticles = NIR fluorescent protein (iRFP) and glucose oxidase (GO*x*) were collectively deployed as the templates for the biomineralization of Mn^{2+} and as a NIR fluorescent nanoprobe. [b]GO*x*@Au@$MagSiO_2$ = glucose oxidase immobilized Au nanoparticle-attached magnetic SiO_2.

Table 3. Comparative Data of NIR-PADs with Clinical Analysis for Patient Blood Glucose

		glucose concentration (mM)		
no.	patient	hexokinase-glucose-6-phosphate dehydrogenase method (clinical method)	NIR-PADs[a]	R.S.D. (%)[b]
1	diabetic blood	16.4	17.4 ± 0.10	0.57
2		11.6	12.0 ± 0.05	0.42
3		6.56	6.87 ± 0.21	3.06
4		5.50	5.79 ± 0.19	3.28
5		9.28	9.47 ± 0.29	3.06
6		6.72	6.79 ± 0.15	2.21
7		11.3	11.0 ± 0.41	3.73
8		7.78	7.35 ± 0.10	1.36
9		8.89	8.81 ± 0.11	1.25
10	non-diabetic blood	4.67	4.86 ± 0.03	0.62
11		4.33	4.49 ± 0.11	2.45
12		4.78	4.96 ± 0.07	1.41
13		4.56	4.60 ± 0.04	0.87
14		4.56	4.68 ± 0.03	0.64
15		4.78	4.93 ± 0.26	5.27
16		5.17	4.86 ± 0.08	1.65
17		4.06	4.20 ± 0.20	4.76
18		4.83	4.99 ± 0.02	0.40
19		5.61	5.97 ± 0.16	2.68

[a]N = 3. [b]R.S.D.: relative standard deviation.

To construct the calibration curve and evaluate its quantification performance between glucose concentration and increased emission intensity, the dynamic emission change curve for a set of 50 replicates of standard glucose concentrations of 0−200 mM was measured (see Figure 4). The Tukey statistical estimate was incorporated into the filter process to find the outliers for each concentration. After the removal of the outliers, the linear regression model between 1 and 30 mM was [relative emission intensity] = 0.0451 + 0.0250[glucose] (Figure S3). The regression coefficient of 0.025 (95% confidence interval 0.02−0.03, P-value < 0.001) represented the mean change in the relative emission change variable for one unit of change in the predictor glucose concentration variable. The model fitting was good (R^2 = 0.9984) with the limit of detection (LOD); S/N = 3 was 0.7 mM. The normality assumption was evaluated based on the Shapiro−Wilk normality test (p-value = 0.2945). The Durbin−Watson test had a null hypothesis that the autocorrelation of the disturbances was 0 (P-value = 0.1677). This shows that this model fits well.

After processing the data with R programming, the glucose sensing range of **NIR-PADs** in the calibration curve could

https://doi.org/10.1021/acsomega.1c04344
ACS Omega 2022, 7, 198−206

detect patients with and without diabetes. We also compared the analytical performances of the recent direct glucose detection sensors in human whole blood systems (Table 2). The results demonstrated that **NIR-PADs** have better glucose detection conditions by the luminescence methodology without blood sample pretreatment and a dilution factor.

The effects of interference by interferents, such as D-(−)-fructose, L-(+)-ascorbic acid, D-(+)-galactose, several ions, D-maltose, and so forth, were tested with **NIR-PADs** (Figure S4). Interestingly, none of the interferents showed interference for the system. This further indicates the outstanding selectivity of the new **NIR-PADs** for glucose sensing in whole blood.

In the human blood analysis, **NIR-PAD** results and clinical results on blood from 19 patients were compared (Table 3 and Figure 5). The relative standard deviation (R.S.D) of **NIR-PADs** for all the patients ranged from 0.40 to 5.27%. The accuracy of the sensor was confirmed. In addition, a significant correlation between the data generated by the two methods was achieved (r = 0.993 and p = 0.0105, Figure 5). It can be seen that the results obtained from these two methods presented similar diagram patterns. We additionally determined the mean absolute relative difference (MARD) of all paired points. The MARD for **NIR-PAD** measurements across all values (N = 19) was 3.64%, indicating that the **NIR-PAD** readings were close to the clinical glucose value.

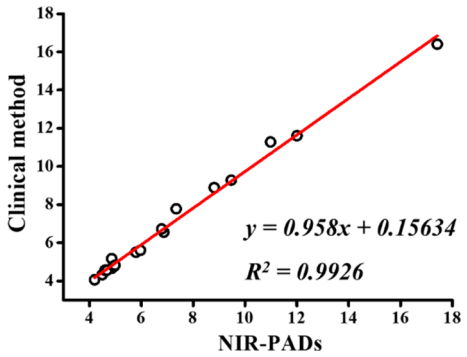

Figure 5. Correlation plot of two detection methods, **NIR-PADs** and clinical method. The units for both axes are millimoles.

To confirm the stability of the **NIR-PADs**, we conducted glucose measurements after storage for 1 month at 4 °C. The percent errors of the sensor after 1 month were <0.06%, indicating that **NIR-PADs** have good stability and that the 3D gel can protect the enzymes from denaturation during storage (Figure S5).

In the present study, we proposed a new method to determine the glucose concentration in human whole blood by using NIR metal complexes as the phosphorescent probes. The data were treated with the programming language R to construct a calibration curve to filter the outliers. The performance of the sensor is comparable to those of clinical methods of glucose detection.

The findings in our results were three-fold. First, we observed different reactional mechanisms and abilities between oxygen and the three NIR probes. Second, we observed that **NIR-PADs** have good sensing ability to glucose in human whole blood. The linear response is shown over the entire physiologically relevant concentration range (Figure 4). To reduce the ambient oxygen dependence of the sensor response in our experiment, we incorporated a control experiment to reduce the effects of the ambient oxygen concentration and the differences between each device.[44] In addition to the 3D gel glucose sensing devices, 3D gel devices without GOx were also prepared as control devices. We measured 50 glucose sensing devices and control devices for each concentration and recorded the luminescence intensities. The response of each glucose device was calibrated with control devices. Then, the relative changes in emission intensity upon addition of different concentrations of glucose were calculated. In addition, to reach more users, R is an open-source programming language and is cross-platform. In other words, anyone can use it freely without any licensing or fees, and it can be used on platforms running Windows, Apple, or Linux operating systems. Third, we observed no significant deviation in glucose measurements derived with **NIR-PADs** from glucose measurements derived with a clinical method.

Since it is also important to detect hypoglycemia in clinical settings, this pilot study enrolled healthy participants and demonstrated that it is feasible for **NIR-PADs** to detect glucose levels of <5 mM. The precision and accuracy of a glucose sensor for detecting glucose levels in hypoglycemia ranges need to be much better than those for high glucose concentrations.[45] Glucose-error grid analysis[45] can be applied in further study to confirm the usefulness of the present method for hypoglycemia detection in diabetic patients.

McShane's group investigated one means of extending the longevity of enzymatic microparticle-based sensors by the coimmobilization of GOx and catalase in the sensor matrix.[46] Catalases play an important protective role in devices, catalyzing the disproportionation of toxic hydrogen peroxide into O_2 and H_2O.[47] As for prolonging the storage lifetime of devices, enzyme catalase can also be incorporated into the devices with further study.

Overall, we developed in this work a near-infrared paper-based analytical device for blood glucose detection, which was based on iridium(III) metal complexes embedded in a three-dimensional (3D) enzyme gel. The advantages of the **NIR-PADs** are as follows:

- environmental advantages of using paper as a substrate for sensing,
- a cost-effective system for pipetting blood to the 3D gel on paper,
- no need for blood sample pretreatment and a dilution factor based on near-infrared phosphors,
- detection in a time-independent manner (i.e., the luminescence intensity is recorded), and
- generation of a more reliable calibration curve through statistical treatment of data to filter the outliers in each glucose concentration, enabling the user to measure glucose values correctly.

CONCLUSIONS

In summary, for human blood glucose detection, we developed a 3D-gel-encapsulated, near-infrared phosphor optical biosensor. Blood is a complex matrix, and direct detection of glucose in human blood by luminescence sensing without pretreatment procedures is still a challenge. Using water-soluble Ir(III) and Pt(II) complexes with near-infrared luminescence ability, a large Stokes shift, and a long luminescence lifetime eliminated the interference by background autofluorescence and visual color interference in the

https://doi.org/10.1021/acsomega.1c04344
ACS Omega 2022, 7, 198−206

whole blood. The optimal preparation conditions of the devices, their sensing performance on patients' glucose levels, and their stability were discussed. We also tried to construct a calibration curve by using statistical estimation to filter the outliers, which would be a more reliable approach for dealing with the performance of analytical devices. Moreover, our near-infrared phosphor-gel-based sensor, the **NIR-PAD**, exhibited remarkable characteristics for glucose detection in comparison to other types of methods, with no need for a blood sample pretreatment or dilution factor. The above results confirmed that this glucose sensor can be put to practical use for glucose detection.

EXPERIMENTAL SECTION

Materials and Blood Samples. Calcium chloride dihydrate was from J.T. Baker. Sodium dihydrogen phosphate and disodium hydrogen phosphate were purchased from Merck. D-Glucose, glucose oxidase (G2133-50 KU; Type VII specific activity >100,000 units/gram solid), sodium alginate (SA), ascorbic acid, citric acid, succinic acid, tartaric acid, uric acid, D-fructose, D-galactose, lactose, maltose monohydrate, sucrose, urea, leucine, valine, methionine, glycine, alanine, tyrosine, phenylalanine, glutathione, and human serum albumin were from Sigma-Aldrich. The platinum and iridium complexes (**Pt4***, **Ir1***, and **Ir2***) were synthesized according to the published procedure.[11] Advantec filter paper (no. 5C) was produced by Toyo Roshi Kaisha. The blood samples were obtained from adult participants enrolled at Taipei Veterans General Hospital; the details are described in the Human Blood Analysis section. The samples were stored at 4 °C in Vacutainer test tubes containing NaF/K_3 EDTA and were measured for glucose concentration within 5 days of collection.

Oxygen Sensing and Stern−Volmer Experiments. The iridium and platinum complexes used to prepare the sensors have been completely characterized earlier by using X-ray crystallography, proton NMR, mass spectroscopy, and elemental analysis.[1] A gas mixing system using different partial pressure ratios of nitrogen and oxygen was used to explore the oxygen sensing capability of **Pt4***, **Ir1***, and **Ir2*** in the solid state. Complexes (10^{-3}M) were dissolved in deionized water (DI water), deposited, and dried on cellulose paper. The maximum output flow of gas was 600 mL/min. The emission intensities were measured for the different ratios of oxygen. Using the changes in emission intensity in the various partial pressures of oxygen and nitrogen, the collision relationship between the sample and oxygen was calculated to extract the oxygen quenching constant.

Design and Fabrication of the Paper-Based Device for Glucose Sensing. First, Advantec filter paper (no. 5C) was cut into round pieces with a diameter of 5 mm. Then, sodium alginate in DI water (SA, 40 mg/mL) was heated to 120 °C for 1.5 h to obtain a semitransparent viscid gluey solution. The gluey solution was allowed to cool at room temperature. Glucose oxidase (GO*x*, 14 mg/mL) was mixed into pH 6 phosphate buffer solution (PBS, 10 mM). GOx and SA were combined at a volume ratio of 1:1 and thoroughly mixed until uniform. **Ir2*** (or **Ir1*** and **Pt4***; 10^{-3} M) was dissolved in a mixture of GO*x* and SA. Subsequently, 16 μL of **Ir2*** (or **Ir1*** and **Pt4***) solution was added onto the culture dish, and then 16 μL of calcium chloride solution (0.5 M) was added into the **Ir2*** (or **Ir1*** and **Pt4***) solution. After the substitution of calcium ions for sodium ions, a 3D calcium alginate hydrogel formed and was coated onto the filter paper. The **Ir2*** (or **Ir1*** and **Pt4***) embedded in the 3D calcium alginate hydrogel was used to fabricate the glucose sensor.

Procedure of Glucose Detection with Gel Paper-Based Devices. The setup for obtaining luminescence spectra and the images of paper-based devices were described in our previous report.[48] Briefly, the luminescence spectra and the images of the paper-based devices with **Ir2***, **Ir1***, and **Pt4*** gel, respectively, in human blood and with/without glucose, were captured by 406 nm laser excitation with a 420 nm long-pass filter equipped in a microscope with a video camera (QImage 5.0 RTV) and with a sensitive charge coupled detector (CCD, Princeton Instruments, PI-MAX). After that, the luminescence intensities of the paper-based devices with **Ir2*** gel coatings, namely, **NIR-PADs**, were recorded upon addition of different concentrations of glucose with a CCD system with a bifurcated optical fiber system (QBIF600-UV-VIS, Ocean optics, Largo, Seelze, FL, USA).[49]

Outlier Detection and Models. The procedure for clarification of the standard curves for glucose quantification with **NIR-PADs** and for outlier detection is illustrated in Figure 4. We measured 50 glucose sensing devices for each concentration and recorded the response variables (relative emission intensity change) from 1 to 60 s. We used the Tukey test outlier method (1977)[50] to remove the outliers in the experiment. The main concept of this method is to assume that Q1 is the first interquartile range and Q3 is the third interquartile range and to define an outlier as any observation outside the range [Q1 − 1.5 IQR, Q3 + 1.5 IQR], IQR = Q3 − Q1. Finally, we established a linear regression model of glucose concentration (set as predictor variable X) and percentage of emission change (set as response variable Y).

Human Blood Analysis. In the present study, blood samples from 9 adult patients with diabetes and 10 healthy adult controls were obtained at Taipei Veterans General Hospital in Taiwan under an IRB-approved protocol (2017-12-002CC). Blood samples from each subject were collected into two NaF−K_3EDTA vacutainer tubes. The blood glucose level in the first tube was measured by the hexokinase-glucose-6-phosphate dehydrogenase method in the hospital. In brief, glucose and ATP were catalyzed by hexokinase to form glucose-6-phosphate and ADP, and subsequently, glucose-6-phosphate and $NADP^+$ were converted by glucose-6-phosphate dehydrogenase to produce 6-phosphogluconolactone and NADPH, which were quantitated spectrophotometrically at 340 nm to determine the glucose level in the blood.[51] The blood glucose in the second tube was measured by **NIR-PAD**. Here, 2 μL of whole blood was directly added into the gel of the sensor and the dynamic curve was measured. Then, the relative increase in emission intensity was measured, and the glucose level in human blood was determined according to the calibration curve. The process was performed in triplicate.

Statistical Analysis. The glucose data determined by **NIR-PADs** are presented as the mean ± standard deviation. The Spearman correlation coefficient r was used to assess the correlation between paired results measured by the clinical hexokinase method and **NIR-PADs**. For the two paired variables, linear regression analysis was performed to obtain the coefficient of determination (R-squared or R^2). All of the statistics were analyzed in SPSS software (V18.0) and R software (V4.0.5). A two-tailed p-value <0.05 was considered significant.

The absolute difference (the **NIR-PAD** value minus the clinical hexokinase method value) and the relative absolute

https://doi.org/10.1021/acsomega.1c04344
ACS Omega 2022, 7, 198−206

difference (the absolute difference divided by the clinical hexokinase method value) were analyzed for each matched pair, as has been previously done in another study.[52] The mean of the relative absolute difference (MARD) was calculated at all glucose ranges for **NIR-PADs**.

■ ASSOCIATED CONTENT

Supporting Information

The Supporting Information is available free of charge at https://pubs.acs.org/doi/10.1021/acsomega.1c04344.

Absorption and emission of **Pt4***, **Ir1***, and **Ir2*** in the solid state, optimized experiments, tabulated optimized parameters, calibration curve, interference test, and stability of **NIR-PADs** (PDF)

■ AUTHOR INFORMATION

Corresponding Authors

Sergey P. Tunik − *Institute of Chemistry, St. Petersburg State University, St. Petersburg 198504, Russia;* orcid.org/0000-0002-9431-0944; Email: stunik@inbox.ru

Hui-Wen Lin − *Department of Mathematics, Soochow University, Taipei 111, Taiwan*; Email: hwlin@scu.edu.tw

Sheng-Wei Pan − *Department of Chest Medicine, Taipei Veterans General Hospital, Taipei 11217, Taiwan; School of Medicine, National Yang Ming Chiao Tung University, Taipei 11221, Taiwan*; Email: swpan25@gmail.com

Mei-Lin Ho − *Department of Chemistry, Soochow University, Taipei 111, Taiwan;* orcid.org/0000-0001-6315-1832; Email: meilin_ho@gm.scu.edu.tw

Authors

Hsia-An Lee − *Department of Chemistry, Soochow University, Taipei 111, Taiwan*

Peng-Yi Lin − *Department of Chemistry, Soochow University, Taipei 111, Taiwan*

Anastasia I. Solomatina − *Institute of Chemistry, St. Petersburg State University, St. Petersburg 198504, Russia;* orcid.org/0000-0001-7169-1978

Igor O. Koshevoy − *Department of Chemistry, University of Eastern Finland, Joensuu 80101, Finland;* orcid.org/0000-0003-4380-1302

Complete contact information is available at: https://pubs.acs.org/10.1021/acsomega.1c04344

Notes

The authors declare no competing financial interest.

■ ACKNOWLEDGMENTS

The research was supported by Russian Science Foundation (grant no. 19-13-00132, synthesis, characterization, and preliminary photophysical studies of platinum and iridium complexes, S.P.T. and A.I.S.) and the Ministry of Science and Technology, Taiwan.

■ REFERENCES

(1) Saeedi, P.; Petersohn, I.; Salpea, P.; Malanda, B.; Karuranga, S.; Unwin, N.; Colagiuri, S.; Guariguata, L.; Motala, A. A.; Ogurtsova, K.; Shaw, J. E.; Bright, D.; Williams, R. Global and regional diabetes prevalence estimates for 2019 and projections for 2030 and 2045: Results from the International Diabetes Federation Diabetes Atlas, 9 th edition. *Diabetes Res. Clin. Pract.* **2019**, *157*, 107843−107853.

(2) Liu, Y.; Tu, D.; Zheng, W.; Lu, L.; You, W.; Zhou, S.; Huang, P.; Li, R.; Chen, X. A strategy for accurate detection of glucose in human serum and whole blood based on an upconversion nanoparticles-polydopamine nanosystem. *Nano Res.* **2018**, *11*, 3164−3174.

(3) Lee, P.-C.; Li, N.-S.; Hsu, Y.-P.; Peng, C.; Yang, H.-W. Direct glucose detection in whole blood by colorimetric assay based on glucose oxidase-conjugated graphene oxide/MnO_2 nanozymes. *Analyst* **2019**, *144*, 3038−3044.

(4) Cai, Y.; Wei, Z.; Song, C.; Tang, C.; Han, W.; Dong, X. Optical nano-agents in the second near-infrared window for biomedical applications. *Chem. Soc. Rev.* **2019**, *48*, 22−37.

(5) Sordillo, L. A.; Pu, Y.; Pratavieira, S.; Budansky, Y.; Alfanoa, R. R. Deep optical imaging of tissue using the second and third near-infrared spectral windows. *J. Biomed. Opt.* **2014**, *19*, 056004.

(6) Yu, M.; Zhao, K.; Zhu, X.; Tang, S.; Nie, Z.; Huang, Y.; Zhao, P.; Yao, S. Development of near-infrared ratiometric fluorescent probe based on cationic conjugated polymer and CdTe/CdS QDs for label-free determination of glucose in human body fluids. *Biosens. Bioelectron.* **2017**, *95*, 41−47.

(7) Li, C.-P.; Long, W.-W.; Lei, Z.; Guo, L.; Xie, M.-J.; Lü, J.; Zhu, X.-D. Anionic metal-organic framework as a unique turn-on fluorescent chemical sensor for ultra-sensitive detection of antibiotics. *Chem. Commun.* **2020**, *56*, 12403−12406.

(8) Deng, H.; Liu, H.; Kang, W.; Lei, C.; Nie, Z.; Huang, Y.; Yao, S. Biomineralization synthesis of a near-infrared fluorescent nanoprobe for direct glucose sensing in whole blood. *Nanoscale* **2020**, *12*, 864−870.

(9) Zheng, W.; Huang, P.; Tu, D.; Ma, E.; Zhu, H.; Chen, X. Lanthanide-doped upconversion nano-bioprobes: electronic structures, optical properties, and biodetection. *Chem. Soc. Rev.* **2015**, *44*, 1379−1415.

(10) Ute, R.-G.; Markus, G.; Sara, C.-J.; Roland, N.; Thomas, N. Quantum dots versus organic dyes as fluorescent labels. *Nat. Methods* **2008**, *5*, 763−775.

(11) Solomatina, A. I.; Su, S.-H.; Lukina, M. M.; Dudenkova, V. V.; Shcheslavskiy, V. I.; Wu, C.-H.; Chelushkin, P. S.; Chou, P.-T.; Koshevoy, I. O.; Tunik, S. P. Water-soluble cyclometalated platinum-(ii) and iridium(iii) complexes: synthesis, tuning of the photophysical properties, and in vitro and in vivo phosphorescence lifetime imaging. *RSC Adv.* **2018**, *8*, 17224−17236.

(12) Zhang, G.; Zhang, H.; Gao, Y.; Tao, R.; Xin, L.; Yi, J.; Li, F.; Liu, W.; Qiao, J. Near-Infrared-Emitting Iridium(III) Complexes as Phosphorescent Dyes for Live Cell Imaging. *Organometallics* **2013**, *33*, 61−68.

(13) Ma, D.-L.; Ma, V. P.-Y.; Chan, D. S.-H.; Leung, K.-H.; He, H.-Z.; Leung, C.-H. Recent advances in luminescent heavy metal complexes for sensing. *Coord. Chem. Rev.* **2012**, *256*, 3087−3113.

(14) Lo, K. K.-W.; Choi, A. W.-T.; Law, W. H.-T. Applications of luminescent inorganic and organometallic transition metal complexes as biomolecular and cellular probes. *Dalton Trans.* **2012**, *41*, 6021−6047.

(15) Lo, K. K.-W.; Zhang, K. Y. Iridium(iii) complexes as therapeutic and bioimaging reagents for cellular applications. *RSC Adv.* **2012**, *2*, 12069−12083.

(16) Li, Y.; Wu, Y.; Chen, L.; Zeng, H.; Chen, X.; Lun, W.; Fan, X.; Wong, W.-Y. A time-resolved near-infrared phosphorescent iridium-(iii) complex for fast and highly specific peroxynitrite detection and bioimaging applications. *J. Mater. Chem. B* **2019**, *7*, 7612−7618.

(17) Zhang, D.-Y.; Zheng, Y.; Zhang, H.; Sun, J.-H.; Tan, C.-P.; He, L.; Zhang, W.; Ji, L.-N.; Mao, Z.-W. Delivery of Phosphorescent Anticancer Iridium(III) Complexes by Polydopamine Nanoparticles for Targeted Combined Photothermal-Chemotherapy and Thermal/Photoacoustic/Lifetime Imaging. *Adv. Sci.* **2018**, *5*, 1800581−1800593.

(18) Zach, P. W.; Hofmann, O. T.; Klimant, I.; Borisov, S. M. NIR Phosphorescent Intramolecularly Bridged Benzoporphyrins and Their Application in Oxygen-Compensated Glucose Optode. *Anal. Chem.* **2018**, *90*, 2741−2748.

(19) Kwak, S. K.; Kim, J. H. Statistical data preparation: management of missing values and outliers. *Korean J. Anesthesiol.* **2017**, *70*, 407−411.

(20) Lachaud, C. M.; Renaud, O. A tutorial for analyzing human reaction times: How to filter data, manage missing values, and choose a statistical model. *Appl. Psycholinguist.* **2011**, *32*, 389−416.
(21) Cousineau, D.; Chartier, S. Outliers detection and treatment: a review. *Int. J. Psychol. Res.* **2010**, *3*, 58−67.
(22) Sun, H.; Cui, Y.; Wang, H.; Liu, H.; Wang, T. Comparison of methods for the detection of outliers and associated biomarkers in mislabeled omics data. *BMC Bioinf.* **2020**, *21*, 357.
(23) Estiri, H.; Klann, J. G.; Murphy, S. N. A clustering approach for detecting implausible observation values in electronic health records data. *BMC Med. Inf. Decis. Making* **2019**, *19*, 142.
(24) Ahmadi, A.; Khoshfetrat, S. M.; Kabiri, S.; Fotouhi, L.; Dorraji, P. S.; Omidfar, K. Impedimetric Paper-Based Enzymatic Biosensor Using Electrospun Cellulose Acetate Nanofiber and Reduced Graphene Oxide for Detection of Glucose From Whole Blood. *IEEE Sens. J.* **2021**, *21*, 9210−9217.
(25) Zhang, H.; Chen, Z.; Dai, J.; Zhang, W.; Jiang, Y.; Zhou, A. A low-cost mobile platform for whole blood glucose monitoring using colorimetric method. *Microchem. J.* **2021**, *162*, 105814.
(26) Li, B.; Qi, J.; Fu, L.; Han, J.; Choo, J.; deMello, A. J.; Chen, L. Integrated Hand-powered Centrifugation and Paper-based Diagnosis with Blood-in/Answer-out Capabilities. *Biosens. Bioelectron.* **2020**, *165*, 112282.
(27) Cánovas, R.; Blondeau, P.; Andrade, J. F. Modulating the mixed potential for developing biosensors: Direct potentiometric determination of glucose in whole, undiluted blood. *Biosens. Bioelectron.* **2020**, *163*, 112302.
(28) Kim, D.; Kim, S.; Kim, S. An innovative blood plasma separation method for a paper-based analytical device using chitosan functionalization. *Analyst* **2020**, *145*, 5491−5499.
(29) White, D.; Keramane, M.; Capretta, A.; Brennan, J. D. A paper-based biosensor for visual detection of glucose-6-phosphate dehydrogenase from whole blood. *Analyst* **2020**, *145*, 1817−1824.
(30) Liu, P.; Li, B.; Fu, L.; Huang, Y.; Man, M.; Qi, J.; Sun, X.; Kang, Q.; Shen, D.; Chen, L. Hybrid Three Dimensionally Printed Paper-Based Microfluidic Platform for Investigating a Cell's Apoptosis and Intracellular Cross-Talk. *ACS Sens.* **2020**, *5*, 464−473.
(31) Mani, N. K.; Das, S. S.; Dawn, S.; Chakraborty, S. Electrokinetically driven route for highly sensitive blood pathology on a paper-based device. *Electrophoresis* **2020**, *41*, 615−620.
(32) He, X.; Chang, S. J.; Settu, K.; Chen, C.-J.; Liu, J.-T. An anti-HCT-interference glucose sensor based on a fiber paper-based screen-printed carbon electrode. *Sens. Actuators, B* **2019**, *297*, 126763.
(33) Park, C.; Kim, H.-R.; Kim, S.-K.; Jeong, I.-K.; Pyun, J.-C.; Park, S. Three-Dimensional Paper-Based Microfluidic Analytical Devices Integrated with a Plasma Separation Membrane for the Detection of Biomarkers in Whole Blood. *ACS Appl. Mater. Interfaces* **2019**, *11*, 36428−36434.
(34) Sun, X.; Li, B.; Tian, C.; Yu, F.; Zhou, N.; Zhan, Y.; Chen, L. Rotational paper-based electrochemiluminescence immunodevices for sensitive and multiplexed detection of cancer biomarkers. *Anal. Chim. Acta* **2018**, *1007*, 33−39.
(35) Cheng, Y.-H.; Belyaev, A.; Ho, M.-L.; Koshevoy, I. O.; Chou, P.-T. The distinct O2 quenching mechanism between fluorescence and phosphorescence for dyes adsorbed on silica gel. *Phys. Chem. Chem. Phys.* **2020**, *22*, 27144−27156.
(36) Shikuku, V. O.; Zanella, R.; Kowenje, C. O.; Donato, F. F.; Bandeira, N. M. G.; Prestes, O. D. Single and binary adsorption of sulfonamide antibiotics onto iron-modified clay: linear and nonlinear isotherms, kinetics, thermodynamics, and mechanistic studies. *Appl. Water Sci.* **2018**, *8*, 175.
(37) Imla Syafiqah, M. S.; Yussof, H. W. Kinetics, isotherms, and thermodynamic studies on the adsorption of mercury (ii) ion from aqueous solution using modified palm oil fuel ash. *Mater. Today: Proc.* **2018**, *5*, 21690−21697.
(38) Pan, Z.-B.; Wang, Y.-C.; Chakkaradhari, G.; Zhu, J. F.; He, R.-Y.; Liu, Y.-C.; Hsu, C.-H.; Koshevoy, I. O.; Chou, P.-T.; Pan, S.-W.; Ho, M.-L. A silver metal complex as a luminescent probe for enzymatic sensing of glucose in blood plasma and urine. *Dalton Trans.* **2018**, *47*, 8346−8355.
(39) Mao, Y.; Liu, Z.; Liang, L.; Zhou, Y.; Qiao, Y.; Mei, Z.; Zhou, B.; Tian, Y. Silver Nanowire-Induced Sensitivity Enhancement of Optical Oxygen Sensors Based on AgNWs-Palladium Octaethylporphine-Poly(methyl methacrylate) Microfiber Mats Prepared by Electrospinning. *ACS Omega* **2018**, *3*, 5669−5677.
(40) Wu, T.; Liu, Y.; Tang, W.; Li, X.; Yu, Y.; Liu, X. Constraint genetic algorithm and its application in sintering proportioning. *IOP Conf. Ser.: Mater. Sci. En* **2017**, *231*, 012022.
(41) Lee, P.; Rogers, M. A. Effect of calcium source and exposure-time on basic caviar spherification using sodium alginate. *Int. J. Gastron. Food Sci.* **2012**, *1*, 96−100.
(42) Zijlstra, W. G.; Buursma, A. Spectrophotometry of Hemoglobin: Absorption Spectra of Bovine Oxyhemoglobin, Deoxyhemoglobin, Carboxyhemoglobin, and Methemoglobin. *Comp. Biochem. Physiol.* **1997**, *118*, 743−749.
(43) Gökçal, B.; Kip, Ç.; Tuncel, A. One-pot, direct glucose detection in human whole blood without using a dilution factor by a magnetic nanozyme with dual enzymatic activity. *J. Alloys Compd.* **2020**, *843*, 156012.
(44) Collier, B. B.; McShane, M. J. Enzymatic Glucose Sensor Compensation for Variations in Ambient Oxygen Concentration. *Proc. SPIE-Int. Soc. Opt. Eng.* **2015**, *8591*, 859104.
(45) Clarke, W. L.; Anderson, S.; Farhy, L.; Breton, M.; Gonder-Frederick, L.; Cox, D.; Kovatchev, B. Evaluating the Clinical Accuracy of Two Continuous Glucose Sensors Using Continuous Glucose-Error Grid Analysis. *Diabetes Care* **2005**, *28*, 2412−2417.
(46) Singh, S.; McShane, M. Enhancing the longevity of micro-particle-based glucose sensors towards 1 month continuous operation. *Biosens. Bioelectron.* **2010**, *25*, 1075.
(47) Bornhoeft, L. R.; Biswas, A.; McShane, M. J. Composite Hydrogels with Engineered Microdomains for Optical Glucose Sensing at Low Oxygen Conditions. *Biosensors* **2017**, *7*, 8.
(48) Chen, Y.-T.; Lin, C.-Y.; Lee, G.-H.; Ho, M.-L. Four new lead(ii)-iridium(iii) heterobimetallic coordination frameworks: synthesis, structures, luminescence and oxygen-sensing properties. *CrystEngComm* **2015**, *17*, 2129−2140.
(49) Luo, J.-J.; Pan, S.-W.; Yang, J.-H.; Chang, T.-L.; Lin, P.-Y.; Wu, C.-L.; Liu, W.-F.; Huang, X.-R.; Koshevoy, I.; Chou, P.-T.; Ho, M.-L. Detecting glucose levels in blood plasma and artificial tear by au(I) Complex on the carbopol polymer: A microfluidic paper-based method. *polymers* **2018**, *10*, 1001.
(50) Tukey, J. W. *Exploratory Data Analysis*; Addison-Wesley, 1997.
(51) Lin, K.-C.; Tsai, S.-T.; Lin, H.-Y.; Chou, P. Different progressions of hyperglycemia and diabetes among hyperuricemic men and women in the kinmen study. *J. Rheumatol.* **2004**, *31*, 1159−1165.
(52) Akintola, A. A.; Noordam, R.; Jansen, S. W.; de Craen, A. J.; Ballieux, B. E.; Cobbaert, C. M.; Mooijaart, S. P.; Pijl, H.; Westendorp, R. G.; van Heemst, D. Accuracy of Continuous Glucose Monitoring Measurements in Normo-Glycemic Individuals. *PLoS One* **2015**, *10*, No. e0139973.

https://doi.org/10.1021/acsomega.1c04344
ACS Omega 2022, 7, 198−206